

NRC Publications Archive Archives des publications du CNRC

Deep precision machining of SiC ceramics by picosecond laser ablation

Amsellem, W.; Yazdani Sarvestani, H.; Pankov, V.; Martinez-Rubi, Y.; Gholipour, J.; Ashrafi, B.

This publication could be one of several versions: author's original, accepted manuscript or the publisher's version. / La version de cette publication peut être l'une des suivantes : la version prépublication de l'auteur, la version acceptée du manuscrit ou la version de l'éditeur.

For the publisher's version, please access the DOI link below. / Pour consulter la version de l'éditeur, utilisez le lien DOI ci-dessous.

Publisher's version / Version de l'éditeur:

<https://doi.org/10.1016/j.ceramint.2022.11.129>

Ceramics International, 49, 6, pp. 9592-9606, 2022-11-15

NRC Publications Archive Record / Notice des Archives des publications du CNRC :

<https://nrc-publications.canada.ca/eng/view/object/?id=adb3f425-0cfb-4253-979e-cb6d716496d5>

<https://publications-cnrc.canada.ca/fra/voir/objet/?id=adb3f425-0cfb-4253-979e-cb6d716496d5>

Access and use of this website and the material on it are subject to the Terms and Conditions set forth at

<https://nrc-publications.canada.ca/eng/copyright>

READ THESE TERMS AND CONDITIONS CAREFULLY BEFORE USING THIS WEBSITE.

L'accès à ce site Web et l'utilisation de son contenu sont assujettis aux conditions présentées dans le site

<https://publications-cnrc.canada.ca/fra/droits>

LISEZ CES CONDITIONS ATTENTIVEMENT AVANT D'UTILISER CE SITE WEB.

Questions? Contact the NRC Publications Archive team at

PublicationsArchive-ArchivesPublications@nrc-cnrc.gc.ca. If you wish to email the authors directly, please see the first page of the publication for their contact information.

Vous avez des questions? Nous pouvons vous aider. Pour communiquer directement avec un auteur, consultez la première page de la revue dans laquelle son article a été publié afin de trouver ses coordonnées. Si vous n'arrivez pas à les repérer, communiquez avec nous à PublicationsArchive-ArchivesPublications@nrc-cnrc.gc.ca.

Deep Precision Machining of SiC Ceramics by Picosecond Laser Ablation

W. Amsellem¹, H. Yazdani Sarvestani¹ⁱ, V. Pankov², Y. Martinez-Rubi³, J. Gholipour¹, B. Ashrafi¹ⁱⁱ

¹*Aerospace Manufacturing Technology Centre, National Research Council Canada, 5145 Decelles Avenue, Montreal, QC H3T 2B2 Canada*

²*Aerospace Manufacturing Technology Centre, National Research Council Canada, 1200 Montreal Road, Ottawa, ON K1A 0R6 Canada*

³*Security and Disruptive Technologies Research Centre, Emerging Technologies Division, National Research Council Canada, 100 Sussex Drive, Ottawa, ON K1A 0R6 Canada*

Abstract

Silicon carbide (SiC) ceramic is becoming widely used in multiple industrial applications, owing to its exceptional high temperature properties. Yet it is still a challenge to machine SiC using traditional means without causing damage due to its high hardness and brittleness. In this study, a subtractive manufacturing technique based on the use of a fiber picosecond laser was employed to remove material from the reaction bonded SiC surface or create micro-patterns with the minimum damage to the surface, maximum surface quality and precision. Multiple laser processing parameters were investigated with the purpose of obtaining deep high-quality cuts with the minimum surface roughness and the minimum amount of the re-deposited material. The heat affected zone was analyzed by grazing angle X-ray diffractometry, cross-sectional scanning electron microscopy, energy dispersive and micro Raman spectroscopy techniques. The cut shape, depth, surface roughness as well as the kerf width and re-deposition height were assessed using a 3D laser scanning microscopy. The optimum values were established for the focal position, the laser power, linear speed, wobble frequency, wobble pattern, and number of passes. This study also identified the processing parameters for shallow and deep high-precision SiC cutting at a material removal rate of $\sim 2 \text{ mm}^3/\text{min}$. The work demonstrated that the developed laser machining process is an efficient subtractive manufacturing tool that can be integrated into the automated precision cutting systems for machining hard ceramic materials such as SiC and alumina.

Keywords: *Laser machining; Silicon carbide; Ablation; Picosecond laser; Surface roughness.*

ⁱ Address correspondence to: hamidreza.yazdani@nrc-cnrc.gc.ca and behnam.ashrafi@nrc-cnrc.gc.ca, Tel: +1 (514) 283-7421.

1. Introduction

A silicon carbide (SiC) ceramic is widely used in the automotive, aerospace, energy sectors, and defense (e.g., ceramic armour plates) due to its outstanding mechanical, chemical, and electrical properties [1-5]. SiC is known for having high hardness, high thermal conductivity, low thermal expansion coefficient and its ability to maintain high strength at high temperatures [6]. Other industrial applications of SiC include corrosion-resistant ceramics [7] and semiconductor materials [8-11]. Most of these applications necessitate high quality micro-machining [12-15]. There are currently multiple proven ways to machine SiC through subtractive manufacturing, mainly by electro-discharge machining (EDM) and also by grinding, diamond turning, jet cutting and laser machining [16]. EDM, grinding and laser machining all offer high material removal rates (MRR), therefore they are preferable for fast machining of large surfaces [17]. EDM machining offers great efficiency, but suffers from the formation of micro-pores and micro-cracks. Diamond turning and grinding both yield great surface finish, but both experience excessive tool wear. This reduces the quality of the cuts over time as cutting tools start bearing wear marks, which means they are not ideal for continuous high-precision machining. Plasma and water jet cutting are both characterized by high MRR and surface quality, but offer poor control of the erosion rate [18]. Laser machining is another non-contact and wear-less machining technique suitable for architecturing the SiC ceramic [19, 20]. This technique does not require external tooling or media to remove the material and can be run in a continuous well-controlled manner with minimum process variations thereby resulting in high-precision cutting [21, 22]. Moreover, conversely to traditional cutting methods, laser processing requires no mechanical force to be applied, thus avoiding damage of the workpiece.

Laser ablating a material consists in removing it by irradiation with a laser beam to cause its vaporization or sublimation. By focusing the correct amount of laser energy on the material's surface it is possible to achieve ablation of SiC with minimum energy consumption and low thermal impact on the original workpiece [23, 24]. Four laser operation modes are currently used in manufacturing: continuous, quasi-continuous, short (nanosecond) and ultra-short (picosecond and femtosecond) laser processing. Because of long interaction time, the first two modes usually result in very large heat affected zones (HAZ) and therefore mainly used for drilling, welding and heat treatments. Short and ultra-short laser processing yields much better results and well suited for precise subtractive manufacturing. Nanosecond laser pulses typically remove the material

through its heating, melting and evaporation while often resulting in unacceptably large heat-affected zones and microcracking. The main difference between short and ultrashort laser machining is that in the former case the laser radiation interacts with the lattice while in the latter case it can only interact with electrons [25]. As a result, the ultra-short laser pulse power is readily absorbed by most of work materials through the “cold” multiphoton absorption process, which breaks interatomic bonds in the material without causing its melting. If well optimized, ultra-short laser machining enables almost immediate material transition from the solid to the vapor thereby significantly minimizing any adverse thermal diffusion and thermal stress effects.

Picosecond pulsed laser machining is characterized by high MRR. However when performed in air, it often results in material cracking, excessive debris formation, re-deposition of the ablated material and formation of heat affected zones (HAZ) [18]. To remediate some of these issues, underwater laser ablation has been studied. Underwater lasering is useful to lower the temperature of the machined specimen and to reduce the amount of generated debris redeposited on the specimen surface [18, 26-29]. The requirement to use water as a medium removes the simplicity and many other advantages of the laser machining technique [27]. Layers of complexity are added to control the water’s impact on the ablation process. Underwater lasering also generally entails poorer cut quality because it results in a larger and less focused laser beam typically leading to a decreased MRR and generation of cracks [18, 27, 28]. Therefore, there is a strong need in improving the dry ablation machining process and by reducing its downsides such as debris generation and HAZ formation. However, little has been researched on the methods to avoid the above complications.

Previous research on dry ablation of SiC was mainly focused on the ablation process and its effects on the ablated surfaces including changes in the surface hardness [30], laser machining of specific structures such as micro-holes [31] and Fresnel’s micro-structures [32]. Individual laser process parameters such as power, were investigated and the quality of the laser ablated cut was analyzed [33]. In order to achieve high efficiency in ablating precise geometries needed for industrial applications, the use of pico-femtosecond duration pulses is required [25, 34]. Longer pulse durations used in nanosecond lasers results in higher MRR, but also cause excessive burning and melting of the laser machined material. These lasers also result in larger HAZ, poorer cut quality and more redeposited debris. Short pulse duration (picosecond laser) and ultra-short pulse duration (femtosecond laser) yield much better results, because a higher proportion of the pulse

energy exceeds the ablation power threshold, which is required for high-precision machining. When using these lasers, less energy contributes to surface heating and thus minimizes the size of the HAZ while maximizing vaporization of the material [25, 34]. CO₂ lasers are rarely used for short pulse duration applications. Neodymium-doped yttrium aluminum garnet (Nd:YAG) lasers manifest poor energy efficiency and beam quality [31, 33, 35]. Fiber lasers, on the other hand, are preferable for their excellent short and ultra-short duration pulses and higher efficiencies, without the need for an inert gas atmosphere [36]. In order to develop a subtractive manufacturing tool for SiC laser machining to its fullest potential, fiber laser in the picosecond range with a complete parametric study is required to obtain the maximum MRR and the minimum HAZ size. Accordingly, in this study, a picosecond laser ablation in air including optimization of the process parameters (i.e., wobble amplitude, wobble frequency, power, linear speed and number of passes) is explored to ensure defect-free ablation of SiC with the minimum size of the HAZ and the smallest amount of debris.

Silicon carbide components are mainly formed in two ways, reaction bonding and sintering. Each forming method greatly affects the end microstructure as well as mechanical and high-temperature properties of the fabricated components. Therefore, it is reasonable to expect that the machinability of these types of SiC by conventional and laser-based techniques might differ significantly and a thorough optimization of multiple process parameters is required in order to create micro-patterns with the minimum damage to the surface, maximum surface quality and precision for each type of SiC. In the previous studies [22, 37], the optimum process parameters were established for deep laser cutting of alumina. In this work, an improved manufacturing setup was explored for precision micromachining of reaction bonded SiC ceramics. Laser process parameters were optimized to achieve smooth and defect-free deep/shallow cutting patterns by utilizing the servo motors in the laser head. The optimized equipment setup was aimed at removing any melted or vaporized material included a cooling system, dust collector, and vacuum environment. The developed subtractive manufacturing platform maximized MRR and further minimized the size of the HAZ and the amount of deposits to produce customizable accurate cut geometries. This subtractive manufacturing platform facilitated production of architected SiC ceramics with improved mechanical properties thereby warranting a new state-of-the-art engineering for high temperature/impact applications of the SiC ceramics in various industrial applications [38, 39].

2. Experimental Procedure

2.1. Laser machining procedure

In this study, ceramic tiles with dimensions of $50 \times 50 \times 10 \text{ mm}^3$ made of reaction bonded SiC material with a hardness, density, and purity of 26 GPa, 3150 kg/m^3 , and 99%, respectively were procured from Ortech Advanced Ceramics (see Fig. 1). An Ytterbium picosecond fiber laser (YLPP-25-3-50-R) from IPG Photonics with the minimum laser beam width of $17\text{-}20 \text{ }\mu\text{m}$ was used for machining SiC. It delivers 1030 nm wavelength pulses of 3 ps duration and $25 \text{ }\mu\text{J}$ of energy with a repetition rate of up to 1.83 MHz according to a Gaussian spatial profile. This allows to produce a beam with the maximum average energy of 50 W. A laser head manufactured by Aerotech was placed inside a protective chamber within an inert environment, onto a z -stage to allow for different focal positions while maintaining a certain focal position when performing deep cutting, as seen in Fig. 1a. The specimen was placed on a square-shaped holder and secured to it with screws. The specimen holder was placed on an X - Y stage (manufactured by Aerotech) to provide movement of the holder according to the designed pattern. A software provided by IPG Photonics enabled the user to control X - Y - Z movements and micro-positioning of the Aerotech motion controllers. A Keyence IL-300 laser displacement sensor mounted on the laser head allowed the user to monitor the distance between the laser head and the specimen with an accuracy of $\pm 10 \text{ }\mu\text{m}$. This feature was used to determine the specimen z -positions after their exchange. Furthermore, a compressed conical air nozzle was placed above the X - Y stage and used to blow any dust, sparks and fumes away from the specimen surface into a dust collector. The dust collector was placed above the specimen opposite to the air compressor. This helped to achieve a more controlled stable laminar air flow of the cooling air above the specimen surface and avoid re-deposition of dust particles and melted sparks generated during the cutting process. The optimal air pressure was identified after several experimental trials. Cooling down the sample with the air during its cutting was used to reduce formation of micro-cracks and melting of the specimen surface. Within the laser head, two mirrors were mounted on galvo motors to obtain additional precise and ultra-fast motion of the beam onto the sample. This motion can be used with or without the X - Y - Z stage motion, as well as enabling the production of wobble patterns (see Fig. 2b). This helped achieve higher laser scanning speeds with good precision without the need of using the X - Y Aerotech motion controls thereby increasing their longevity. In order to avoid variation in the beam size when tilting the laser beam by the servo motors, an F -Theta lens was employed, which

maintained the tilted beam focus on an imaging plane coinciding with the specimen surface. This lens was utilized for small samples only.

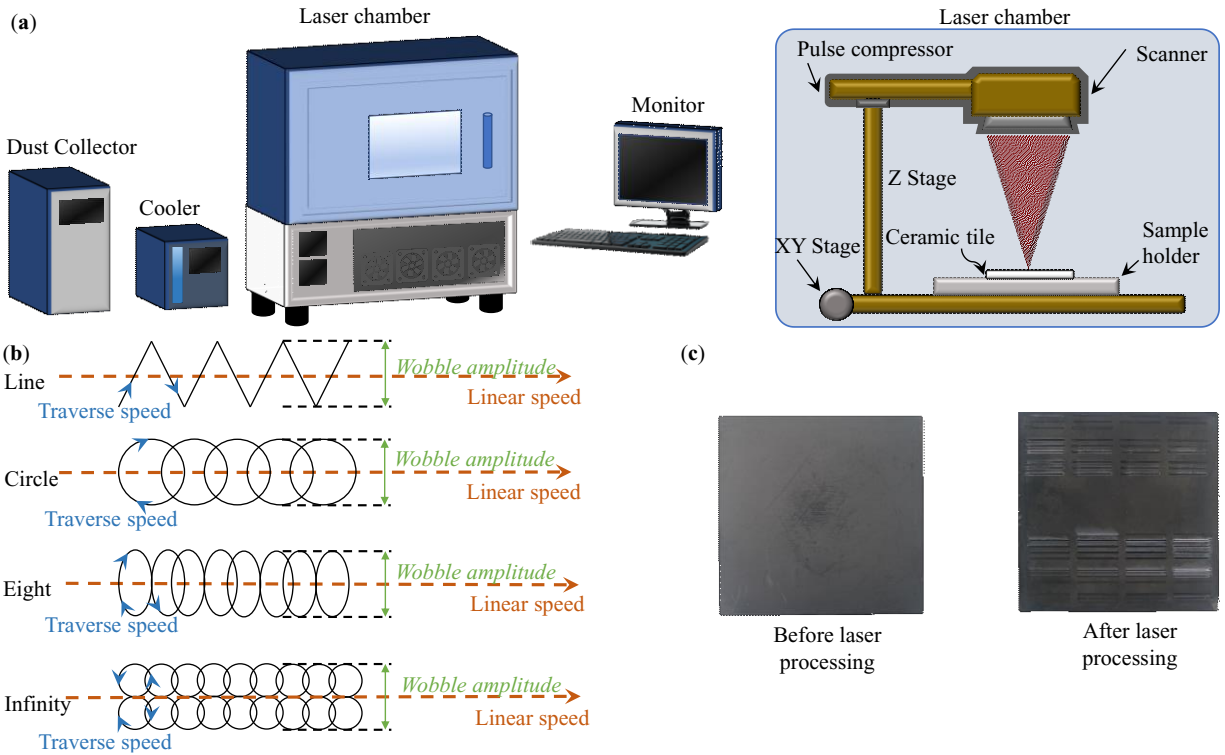


Figure 1: (a) The schematic of the developed subtractive manufacturing system, and (b) Different wobble patterns, and (c) Before and after laser processing on SiC tile.

The power provided by the laser system refers to the overall energy delivered per second by the laser beam. Changing the power is typically achieved by changing the pulse repetition rate (the number of picosecond pulses emitted by the laser per second). The actual pulse duration and energy of each pulse in the laser system cannot be modified and remain constant at around 3 ps and 25 μ J, respectively. The wobble frequency, another important process parameter of the system, defines the repetition rate of each wave pattern. Increasing the wobble frequency reduces the spacing between each performed laser cut while the stage is moving. If a very low wobble frequency is used, then some overlapping consecutively applied cutting patterns occurs. Therefore, one of the objectives of the study was to establish an ideal combination of the linear speed and the wobble speed/wobble frequency in order to obtain a high-quality cut. There are four patterns that can be produced by the galvo motors of the system: straight line, “eight” sign, “infinity” sign, and circle. The energy density was another important process parameter that had to be optimized. The energy

density is defined as the overall energy per second delivered per specific area of the SiC. This parameter is highly dependent on both the power input and the linear speed of the specimen: the faster the *X-Y* stage moves, the less time the SiC is affected by the laser.

2.2. *Focal point and power optimization*

In order to identify the optimum location of the laser focal point with respect to the SiC surface in terms of the MRR and quality of the cut, different *z*-positions of the laser head were evaluated. The cut depth and kerf width were measured by a KEYENCE™ 3D Laser Scanning Confocal Microscope (Keyence VK-X200) and plotted against different focal positions of the laser head with respect to the SiC specimen surface measured as a deviation from the “0” focal position corresponding to the laser beam focal point coinciding with the specimen surface (see Fig. 2a). The data were collected for the laser power values of 5, 10, and 20 W. It was determined that powers less than 5 W offered too insignificant cuts and values above 20 W were too powerful. Indeed, below 5 W, cuts were rarely visible and above 20 W the cuts were so powerful that large white burn marks were visible to the naked eye. As seen in Fig. 2, only the data for the 5 W width curve resemble the bell curve while the MRR shows a significant reduction at the “0” focal position when the laser power is increased to 10-20 W. These data show that at higher laser powers, the energy is not used efficiently when the laser beam is focused on the specimen surface, and the MRR is affected negatively, probably because under these conditions. The laser beam energy goes into melting and redepositing solid particles rather than sublimating the surface. According to Fig. 2, in order to maximize the MRR, the laser beam focus should be repositioned by about 1-1.5 mm above or below the specimen surface.

Another important aspect of laser machining, is the quality of the cut. As seen in Fig. 2c, the quality of the cut is superior at “0” focal position. When the laser is a few mm away from this position, the spread of redeposited material is larger. Instead of vaporizing material at the required area, the material is redeposited further out on each side of the cut. Therefore, if higher powers are needed, then the laser beam must be slightly out of focus in order to maximize the MRR. However, this would not be advisable since the cut quality is reduced considerably and the beam size increases resulting in a larger kerf widths (see Fig. 2a) and probably larger HAZ.

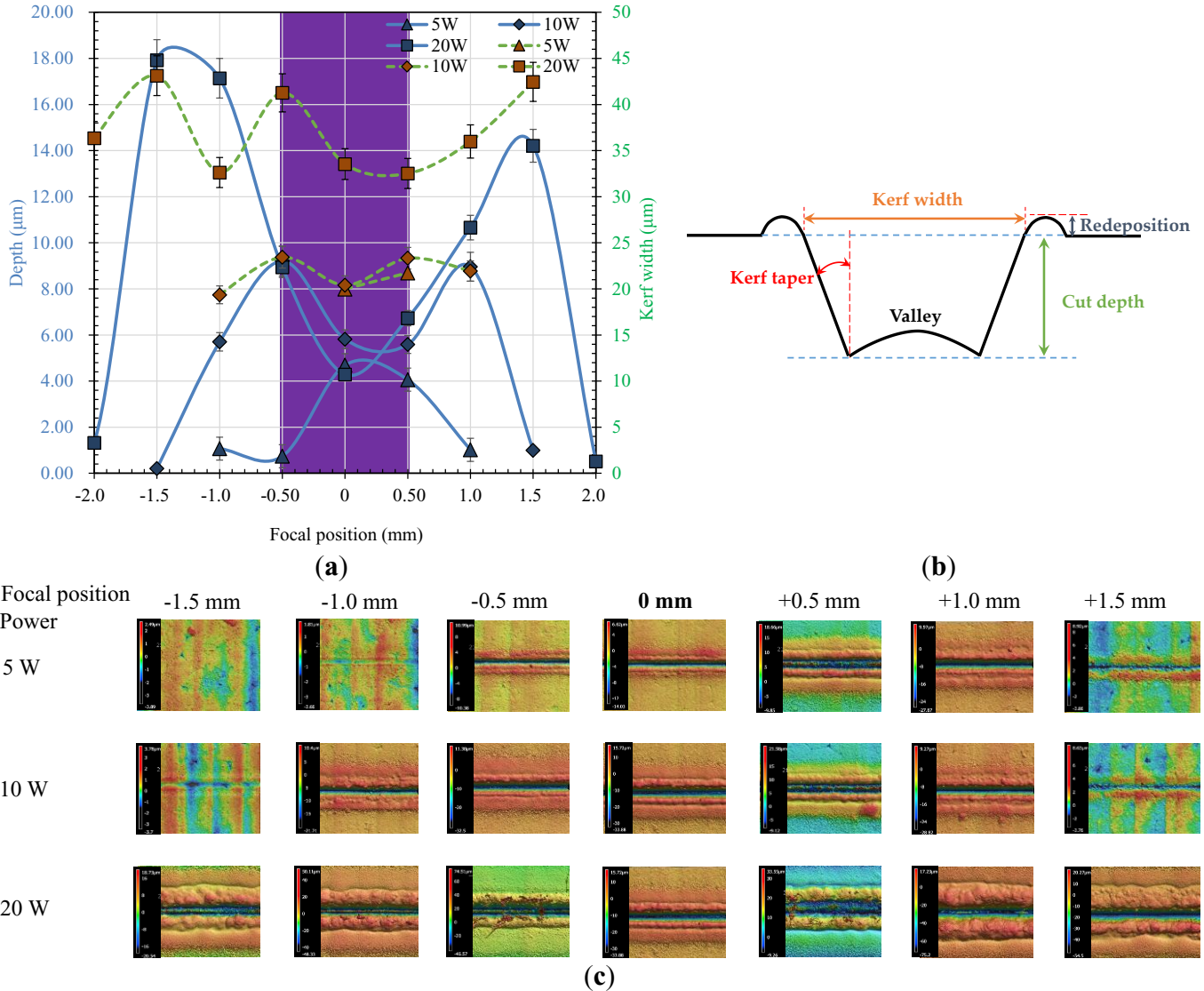


Figure 2: (a) Cut depth and kerf width vs. focal position for the laser powers of 5, 10, and 20 W. “Zero” focal position corresponds to the focal point coinciding with the specimen surface. Negative values of the focal position correspond to the focal point located below the specimen surface. (b) Surface profile and the measurements (side view), and (c) 3D microscopy images for various focal positions (top view).

2.3. Material characterization

The content of crystallographic phases on the surface of SiC specimens before and after laser ablation was analyzed by grazing incidence X-ray diffractometry (GI-XRD) at 3° angle in a Bruker AXS D8 Discovery diffractometer using Cu K α radiation ($\lambda = 0.154056 \text{ nm}$). Phase identification was carried out using the International Centre for Diffraction Data (JCPDS-ICDD 2022) Powder Diffraction Files (PDF).

The internal microstructure of the fabricated specimens was analyzed on cross-sectioned specimens by scanning electron microscopy (SEM) performed in the backscattered electron (BSE)

mode in a Philips XL 30S microscope. Chemical compositional analyses of the fabricated specimens were performed in the SEM using its energy dispersive spectroscopy (EDS) capabilities. Cross-sectional samples were prepared using a standard metallographic specimen preparation procedure based on the cold mounting technique.

Changes in atomic bonding and defect generation at the SiC surface caused by its laser irradiation during machining were analyzed by micro-Raman technique in a Renishaw in Via micro-Raman spectrometer. Samples were measured using a 514 nm excitation laser focused to approximately 1 μm through a 50x objective. The **laser power density was limited to 8 kW/cm²** to prevent conversion of amorphous forms to crystalline forms during spectra acquisition.

3. Results and Discussion

3.1. Effects of laser ablation on SiC material

The effects of laser ablation on the properties of the SiC surface were evaluated under the following laser irradiation conditions: 10 mm/s linear speed, 1000 Hz frequency, 5 W power, 10 passes and 0.5 mm wobble amplitude for micro-Raman and GI-XRD as well as 10 mm/s linear speed, 800 Hz frequency, 10 W power, 10 passes and 0.1 mm wobble amplitude for the cross-sectional SEM.

Figure 3a shows a cross-sectional SEM micrograph of a laser machined groove. The image demonstrates that laser micromachining provides good control of the profile geometry. The figure also revealed the presence of the re-deposited material with a thickness varying within 2-10 μm . Individual layers of the re-deposited material formed after each individual laser pass can be distinguished in a high-magnification image presented in Fig. 3b. Individual particles with dark BSE contrast and a size of about 1-3 μm seen in Fig. 3 consisted of carbon according to the conducted EDS spot analyses. EDS profiling performed across the HAZ (Fig. 3a, Fig. 4 and Table 1) revealed that the ablated subsurface region is enriched with oxygen to a depth of about 3 μm with its concentration reaching about 10 at%. As seen in Table 1, the oxygen content in the re-deposited material is even higher and reaches about 22 at%.

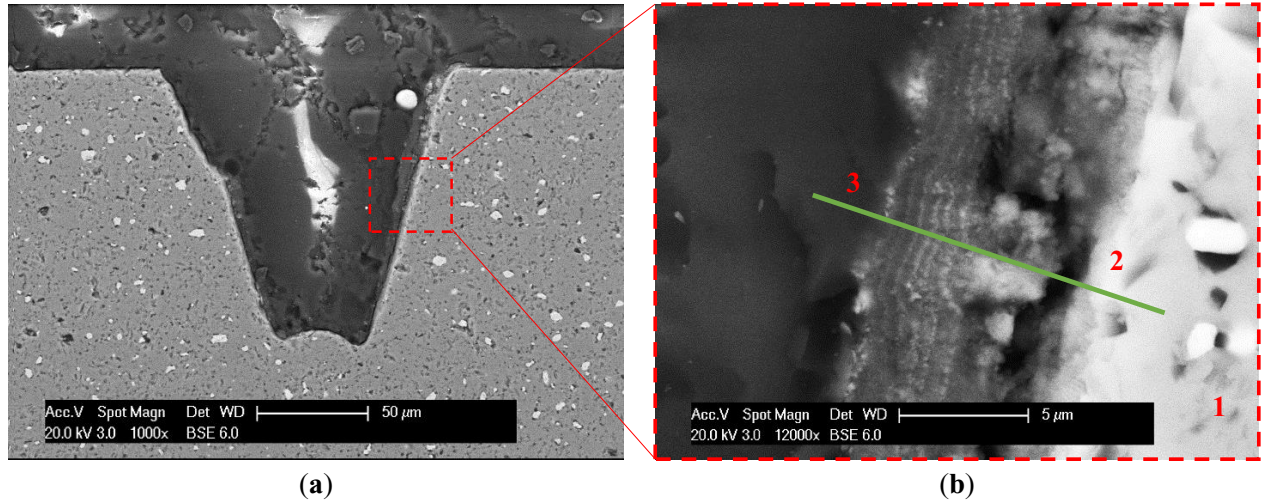


Figure 3: SEM-BSE micrographs of (a) Laser cut made by using 10 passes at 10 W laser power, and (b) a magnified image of the selected area showing multiple layers of the re-deposited material (green line shows the location of the performed EDS line scan).

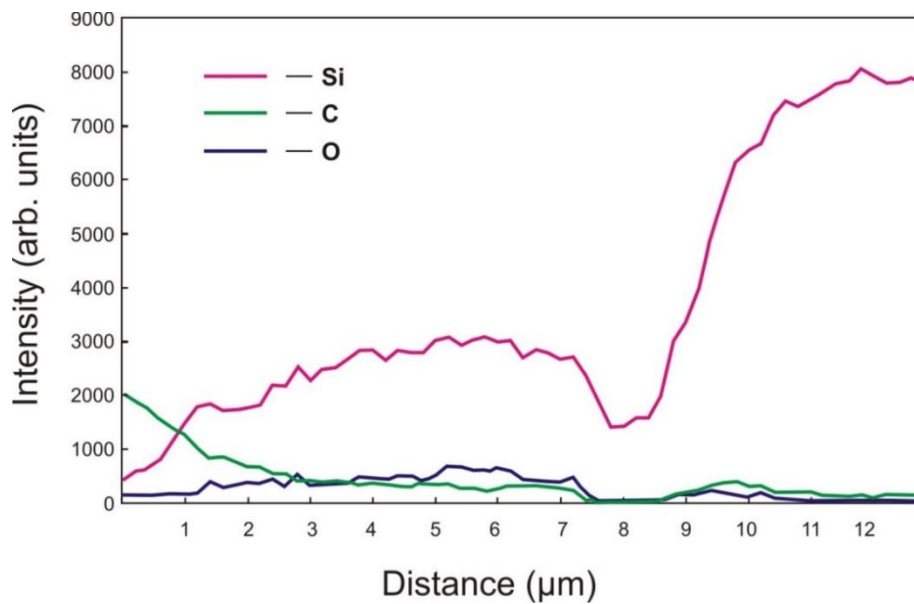


Figure 4: EDS elemental profile along the line scan shown in Fig. 3b.

Table 1: EDS analyses of elemental concentrations in different surface locations of the laser machined specimen (in at%).

Location	Si	C	O
1	45.0	55.0	–
2	21.8	69.0	9.2
3	10.2	68.0	21.8

Figure 5 shows X-ray diffraction patterns of the untreated and laser ablated surfaces. Both patterns look almost identical except a peak at 26.6° which is typically attributed to the family of

planes in the hexagonal lattice of graphite (PDF 00-56-0159) [40]. According to the XRD analyses, the presence of this phase in the subsurface regions of the SiC material drastically reduces as a result of laser irradiation. This can be due to volatilization of free non-reacted carbon particles typically present in the reactive bonded SiC material through its reaction with atmospheric oxygen at high temperature. The remaining peaks closely matched the diffraction patterns from the powder of the hexagonal α -polytype 6H-SiC polytype (PDF 00-29-1131). As seen in Fig. 5, some of the peaks also provided a close fit with the cubic β -polytype 3C-SiC polytype (PDF 00-29-1131) suggesting a possible mix of α - and β -SiC phases. Therefore, Raman spectroscopy was carried out to provide a more accurate identification of the crystalline phases present in the sub-surface region of the untreated and laser ablated SiC specimens.

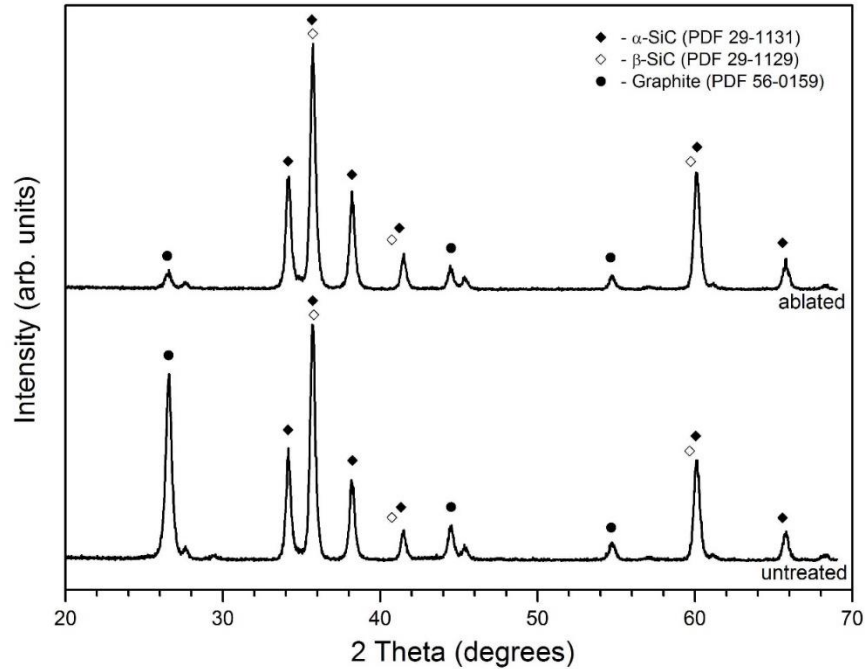


Figure 5: GI-XRD patterns acquired from the untreated and laser machined surfaces of the SiC material.

Raman spectroscopy has often been used to extract various information on the fine structure of the SiC material including identification of the presence of specific polytypes, structural disorder, damage, and generated lattice strain [41-43]. Figure 6 shows Raman spectra collected from the untreated and laser machined areas of the SiC surface. The typical spectra acquired from the pristine SiC surface (marked as “1” in Fig. 3b) contained four peaks characteristic of the hexagonal α -polytype 6H-SiC, which is consistent with the results of the GI-XRD analyses (see

Fig. 5]) while eliminating the possibility of the presence of the cubic β -polytype 3C-SiC in both the untreated and treated SiC material. The peaks at 769 and 789 cm^{-1} were assigned to E_2 (transverse optical, TO) phonon modes and the peak at 969 cm^{-1} was assigned to the A_1 (longitudinal optical, LO) mode [42-44]. The second order Raman peak at 147 cm^{-1} corresponded to E_2 planar or transverse acoustic (TA) mode. Raman spectra collected at certain locations within the untreated area also showed D and G bands associated with carbon phases (see Fig. 6b): the D band is usually attributed to the disorder or polycrystalline carbon and the G band to the graphite-like carbon [45, 46]. The presence of carbon in the reaction bonded untreated SiC is consistent with the results of the GI-XRD analysis presented in Fig. 5.

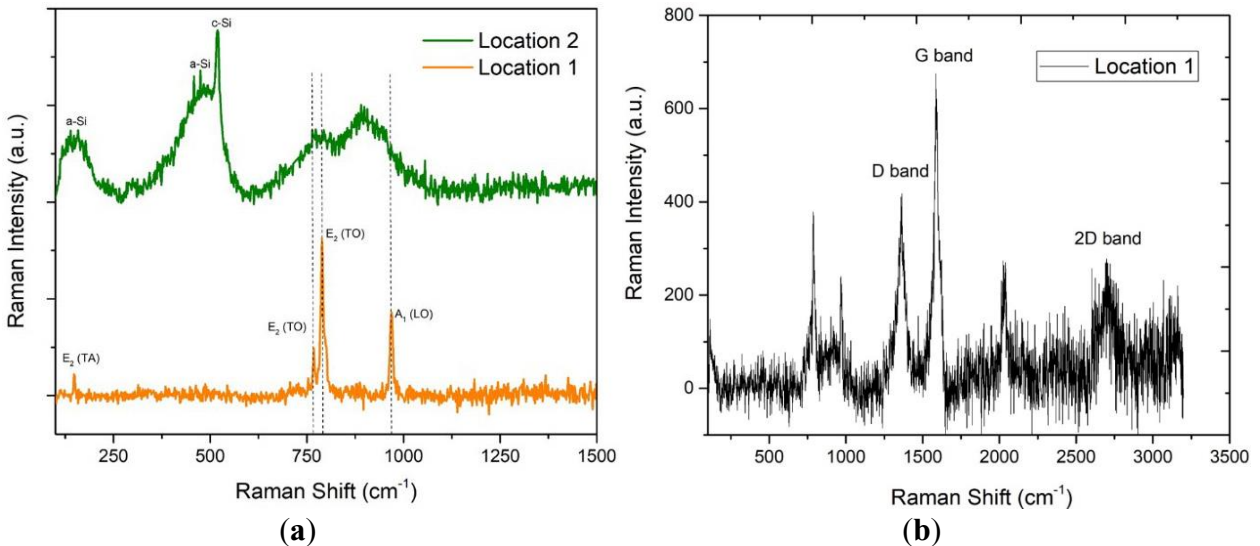


Figure 6: (a) Typical Raman spectra acquired from the untreated (marked as “1”) and laser machined (marked as “2”) areas of the SiC surface, and (b) The spectra collected from some locations within the “1” area showing the presence of carbon.

Figure 6b shows the typical Raman spectrum collected within the laser machined area. Because of the small wavelength of the used excitation laser (514 nm), the expected penetration depth of the laser irradiation in penetration depth in the analyzed specimen is less than 1 μm [47]. Thus, based on the cross-sectional SEM presented in Fig. 3, the collected spectra mainly represent a re-deposited material. Comparison of Raman spectra collected from the laser ablated region with those acquired from the untreated SiC surface shows the disappearance in the former of Raman shift peaks associated with the crystalline 6H-SiC in the 760-975 cm^{-1} region, the appearance of a new peak in the vicinity of 520 cm^{-1} and four broad bands near 155 cm^{-1} , 480 cm^{-1} , 770 cm^{-1} , and 892 cm^{-1} . The peak at 520 cm^{-1} can be assigned to the first-order Raman scattering of the

longitudinal optical (LO) phonon mode for crystalline silicon (c-Si) while the two broad bands near 155 cm^{-1} and 480 cm^{-1} are the characteristic features of the amorphous silicon (a-Si) [45, 46]. The third band located near 770 cm^{-1} can be due to amorphization of the 769 and 789 cm^{-1} characteristic peaks E_2 (TO) of the crystalline 6H-SiC polytype while the fourth broad band centered at around 892 cm^{-1} could be associated with the A1 axial optic mode of 6H-SiC [47]. The disappearance of Raman shift peaks associated with the crystalline SiC and the appearance of wide bands attributed to amorphous silicon in the Raman spectra suggests the possibility of SiC dissociation under laser irradiation and its consecutive Si oxidation in a very thin (about $3\text{ }\mu\text{m}$) sub-surface region.

3.2. Effects of process parameters on cut depth and material re-deposition

When performing cutting using picosecond lasers as opposed to continuous or quasi-continuous lasers, typically used for welding, the kerf width is usually too small resulting in very narrow cuts and some undesirable effects such as excessive material re-deposition. In order to keep the kerf width within the required range, laser wobbling using various patterns and different wobbling parameters has been used in the study. The effects of the following seven laser processing parameters on the cut depth and the thickness of the re-deposited material were evaluated: the focal position (z-height), wobble frequency, wobble pattern, wobble amplitude, number of passes, linear speed, and laser power. The studied linear speed values included 5, 10, 15, and 20 mm/s.

3.2.1. Wobble frequency

The wobble frequency was tested at different linear speeds and laser powers. The number of passes and wobble amplitude are kept 10 and 0.5 mm, respectively. The established relationships were used to eliminate one variable from further consideration while evaluating the remaining variables. As seen in Figs. 7a and 7b, the faster the laser beam moves along the specimen surface, the smaller is the depth of the cut because there is less time to vaporize material. There seems to be no relation between wobble frequency, linear speed and the height of the re-deposition ridge at a laser power of 5 W. The cut depths are visibly the same for different wobble frequencies in the 5-10 W laser power range. The re-deposition heights vary significantly with the laser beam speed and slightly with the wobble frequency. As shown in Fig. 8, the minimum relative re-deposition

height for 5 mm/s occurs at 400 Hz, for 10 mm/s it is at 800 Hz, for 15 mm/s it is 1200 Hz and for 20 mm/s it occurs at 1600 Hz. The wobble frequency-to-speed ratio for the lowest redeposition and highest quality cut was determined to be 80.

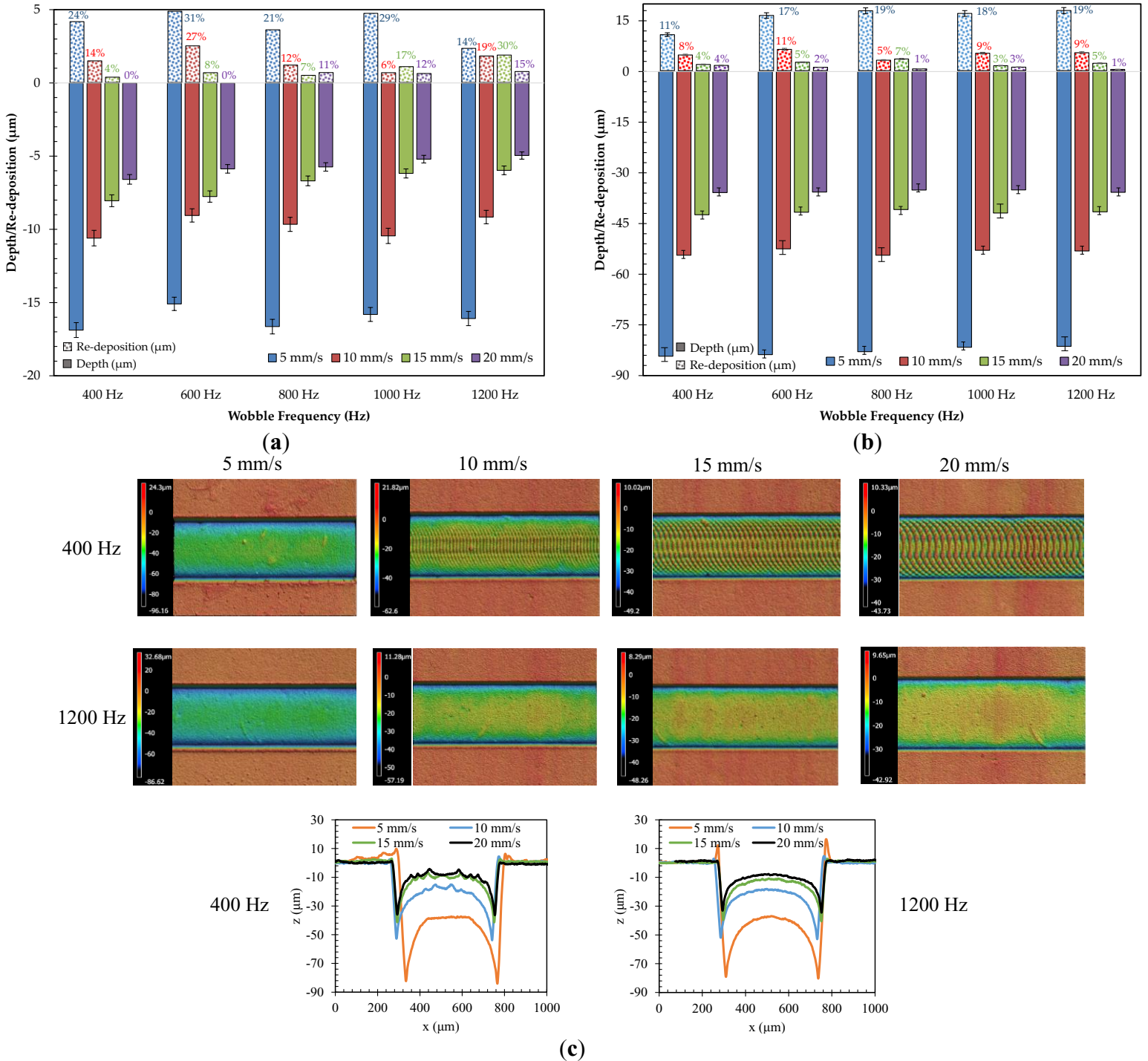


Figure 7: Depth and re-deposition vs. frequency at different speeds with power of (a) 5 W, and (b) 10 W. (c) Top microscopy view of cut profiles (number of passes: 10, wobble amplitude: 0.5 mm).

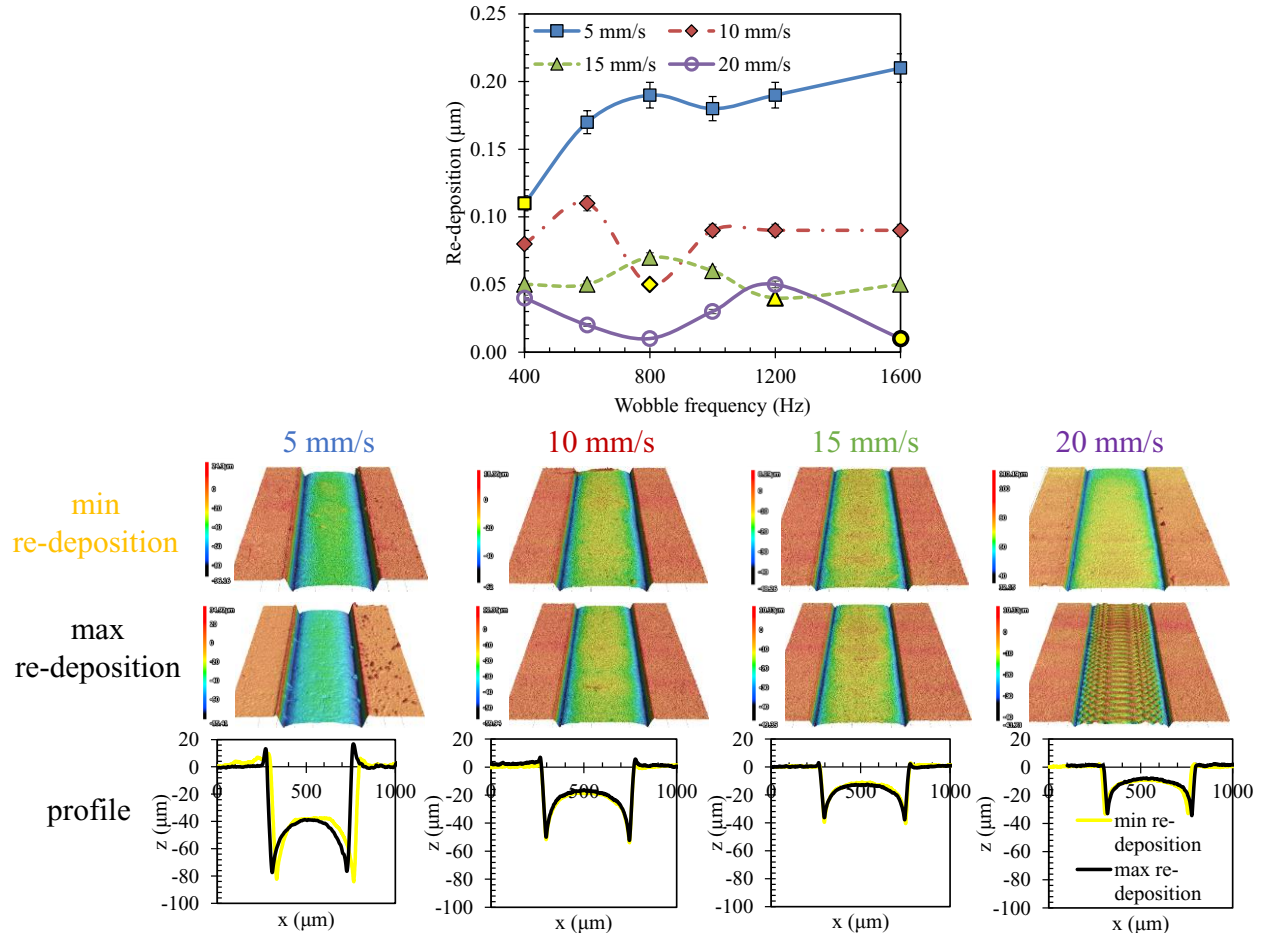


Figure 8: Re-deposition vs. wobble frequency for different linear speed (laser power: 10 W, number of passes: 10, wobble amplitude: 0.5 mm).

Analysis of the effect of the linear speed of the laser beam along the surface on the produced kerf width at different values of the laser beam power revealed that the produced kerf width at 5 W was smaller than that defined in the laser system by the wobble amplitude set to 500 μm (see Fig. 9a). On the contrary, at 10 W the kerf width was larger than the set wobble amplitude value (see Fig. 9b). At a laser power of 5 W, it was unclear how the linear speed of the laser beam affected the kerf width. However, at 10 W, the kerf width increased with increasing linear laser speed. Overall, 10 mm/s at 10 W seems to be the closest to the desired 500 μm kerf width. There does not seem to be any strong correlation between the laser wobble frequency and the produced kerf width. Similarly, for the roughness of the laser-machined surface, a strong correlation was observed with the linear laser speed when using the laser power of 10 W (see Fig. 9d) while no such correlation was observed at the lower power of 5 W (see Fig. 9c). No correlation was revealed between the surface roughness and wobble frequency in the 4 to 15 mm/s while at a speed of 20

mm/s the roughness of the laser-machined surface decreased with increasing wobble frequency. For the remaining experiments, the laser power of 10 W and the wobble frequency-to-speed ratio of 80 were used.

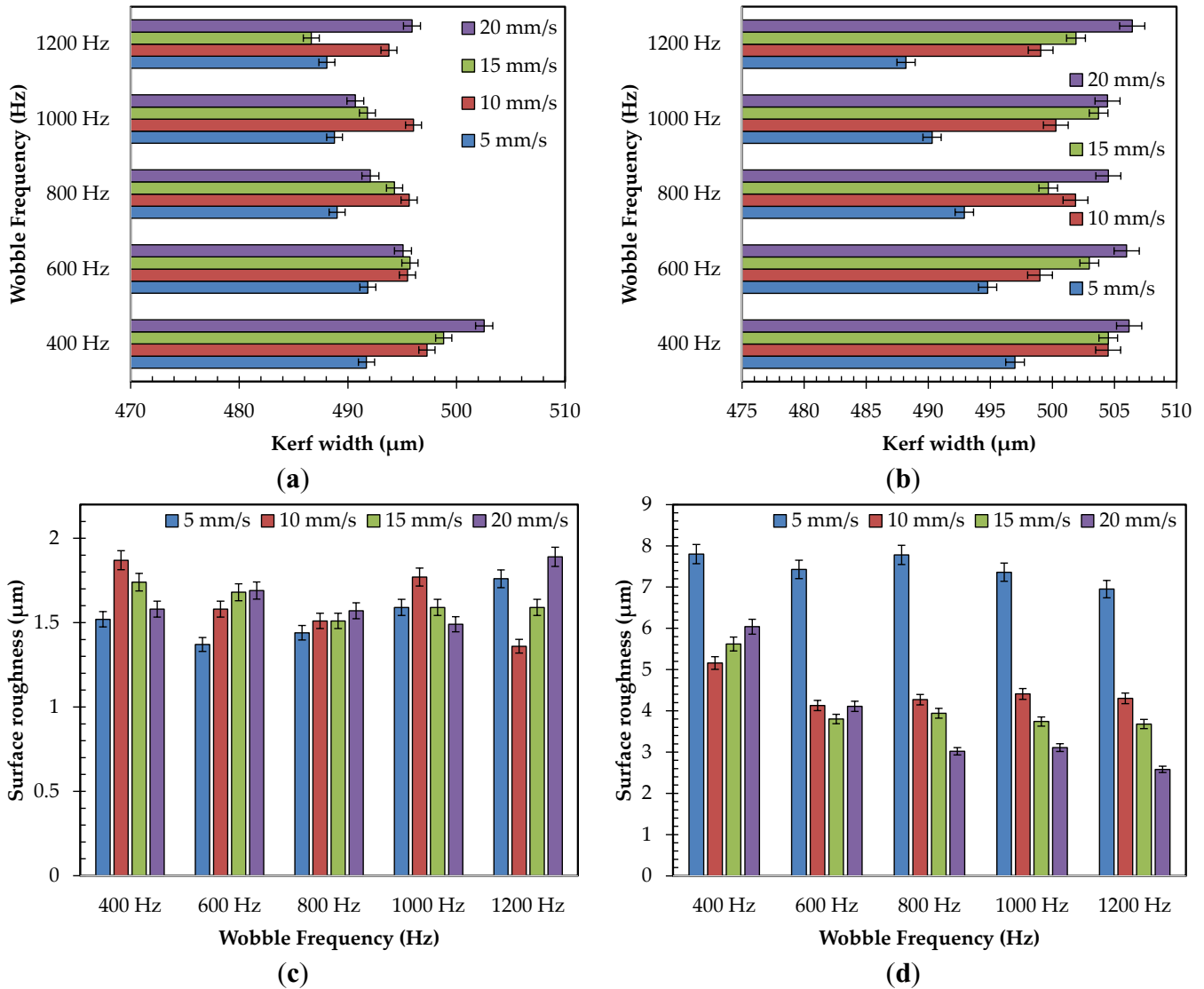
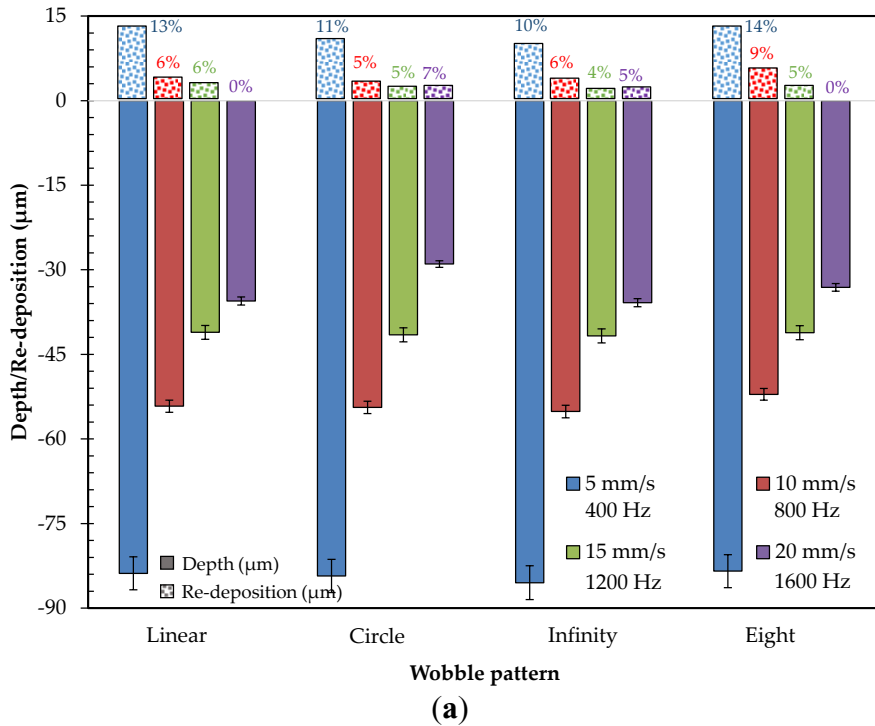


Figure 9: Kerf width vs. frequency at different linear speeds with laser power of (a) 5 W, and (b) 10 W. Surface roughness vs. frequency at different linear speeds with power of (c) 5 W, and (d) 10 W (number of passes: 10, wobble amplitude: 0.5 mm).

3.2.2. Wobble pattern

To study the wobble pattern, the number of passes, wobble amplitude, and laser power are kept 10, 0.5 mm, and 10W, respectively. A strong correlation was observed between the cut depth, re-deposition height, and linear speed for different wobble patterns for all four evaluated wobble

patterns (see Fig. 10a). However, as seen in Fig. 10, for different patterns, the correlation between the re-deposition height and linear speed is more pronounced for the “circle” pattern. There was no noticeable difference in cut depths for different wobble patterns. This was unexpected, since different patterns should incur different linear speeds within the pattern trajectory. The “infinity” and “circle” patterns had the lowest re-deposition heights at lower laser beam linear speeds, while the “linear” and “eight” patterns had no redeposited material at a speed of 20 mm/s and 1600 Hz wobble frequency. No correlation was revealed between wobble patterns and kerf widths (see Fig. 10b), but the most accurate kerf widths (closest to the targeted 500 μm value set in the laser system by the wobble amplitude parameter) were obtained when using the “eight” and “linear” patterns. The “infinity” pattern was found to be the most inaccurate in that regard. As can be seen in Fig. 10c, there was a strong correlation between the laser-machined surface roughness and the linear laser beam speed when using the “circle” and “eight” patterns.



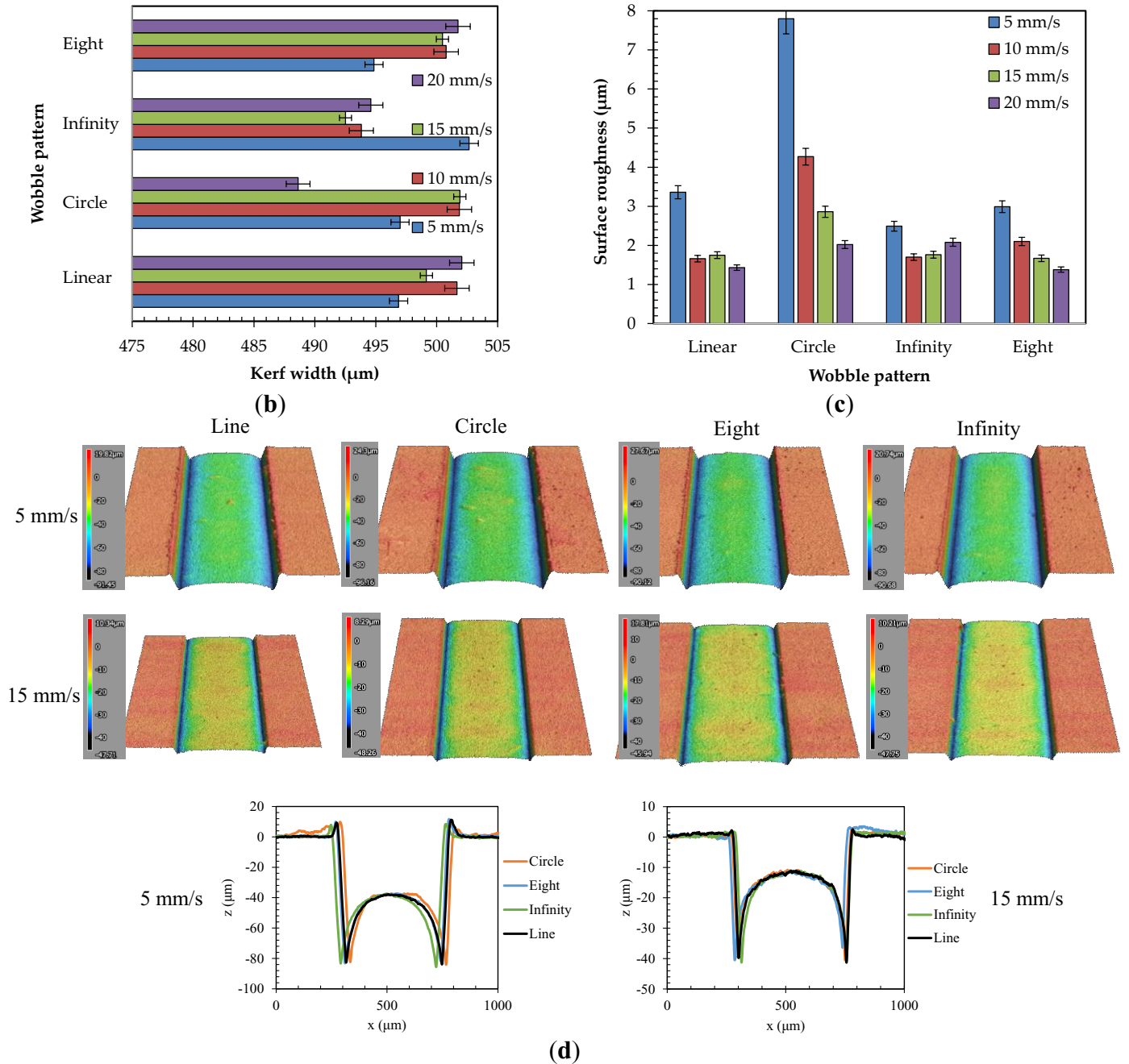
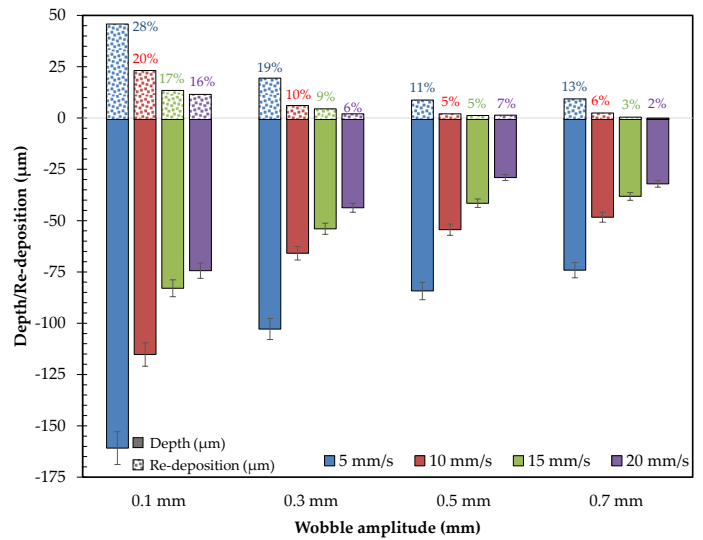
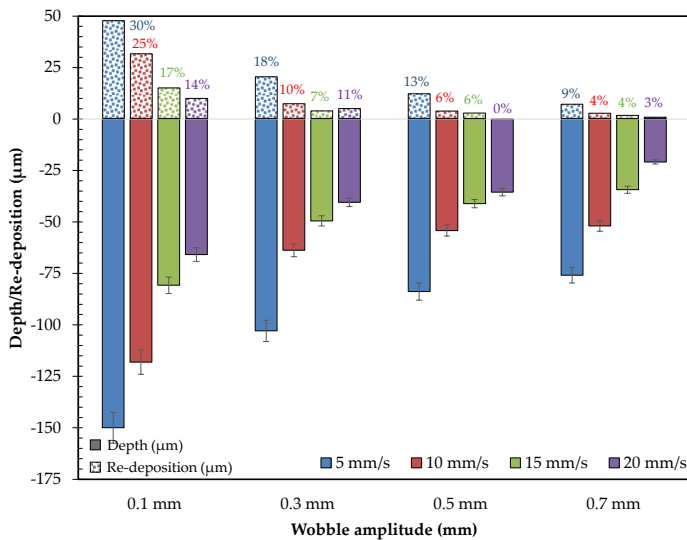


Figure 10: (a) Depth/re-deposition, (b) Kerf width, and (c) Surface roughness vs. wobble pattern at different speeds. (d) 3D microscopy view of cuts with eight, infinity, circle, and line patterns at 5, and 15 mm/s (laser power: 10 W, number of passes: 10, wobble amplitude: 0.5 mm).

3.2.3. Wobble amplitude

The effects of the wobble amplitude on the cut geometry and surface roughness are explored for the “line” and “circle” patterns. The number of passes and laser power are kept 10 and 10 W, respectively. Figures 11 and 12 show that the re-deposition height and kerf width are similar for these two patterns. The roughness of the surface machined using the “circle” pattern is much

smaller than that produced by using the “linear” pattern (see Fig. 12). For the both patterns, the surface roughness increases with as the wobble amplitude and the related kerf width become smaller. For the “line” pattern, the cuts seem to be the smoothest at wobble amplitudes of 0.5-0.7 mm. Reduction in the wobble amplitude resulted in a smaller width of the laser cut, smaller area to ablate, faster material heat-up, higher pressure of the evaporated material and, as a result larger amounts of the re-deposited material (see Fig. 11). A buildup of the re-deposited material at the edges of the cut creates concisions when the laser beam irradiates an inclined surface which is similar to the effect of being out of focus when the beam loses its efficiency and melts the material rather than vaporizing it. This tendency is shown in Fig. 13, which shows the MRR) plotted as a function of the wobble amplitude demonstrating that higher wobble amplitude values result in higher removal rates. The smaller the wobble amplitude and the kerf width, the larger portion of the cut volume is affected by re-deposition and the laser beam defocusing effect. Once the wobble amplitude reaches about 0.3 mm, the MRR value shows a saturation trend since the angled edge represents a smaller part of the overall cut volume. According to Fig. 13, the “linear” wobble pattern maxes out at 1.6 mm³/min while the “circle” pattern continues rising with increasing wobble amplitude. This may be due to a smoother surface roughness near the edges of the cut produced using the “circle” pattern because the galvo motors turn the mirror in circles continuously while spending less time when reaching the “circle” pattern edge than when performing the “line” pattern, which requires the motors to come to an abrupt change in their motion direction each time when reaching the pattern edge.



(a) (b)
Figure 11: Depth/re-deposition vs. wobble amplitude for (a) "line", and (b) "circle" wobble patterns.

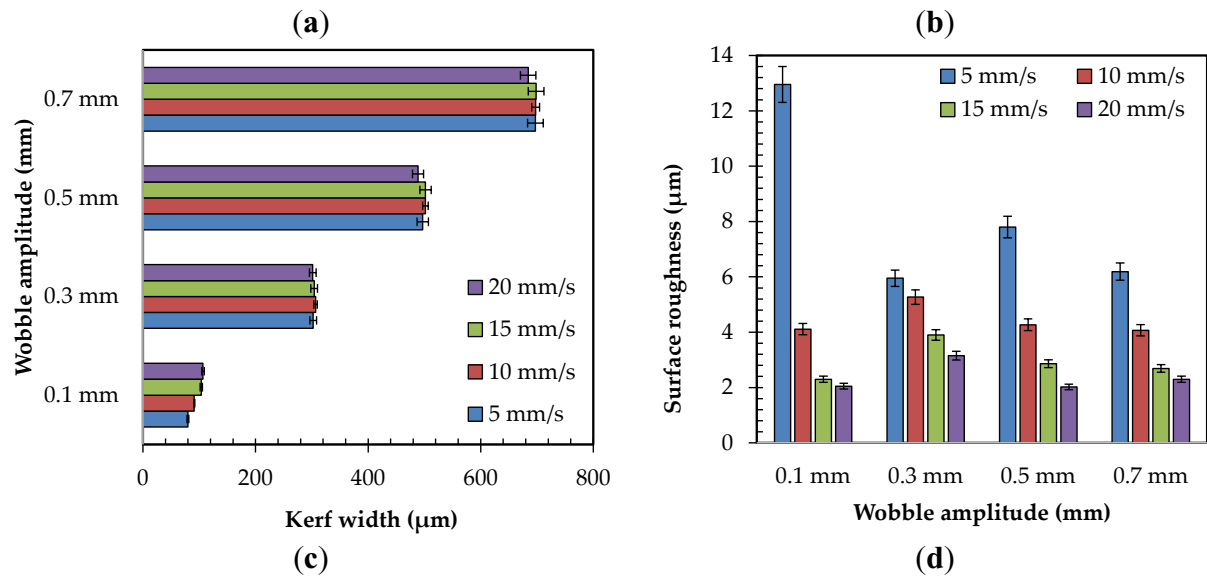
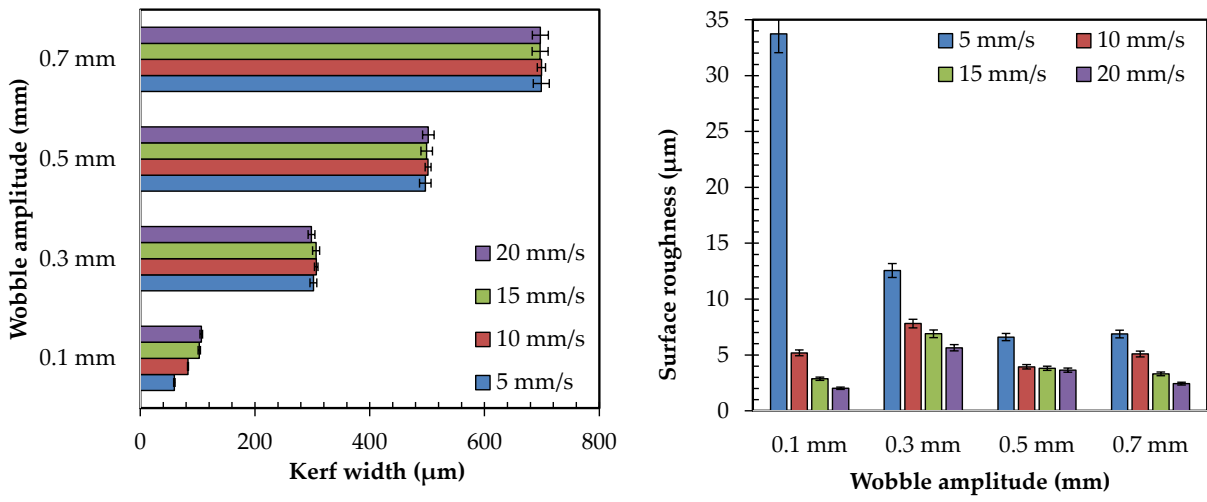


Figure 12: Kerf width and surface roughness vs. wobble amplitude for (a, b) "line" and (c, d) "circle" patterns (laser power: 10 W, number of passes: 10).

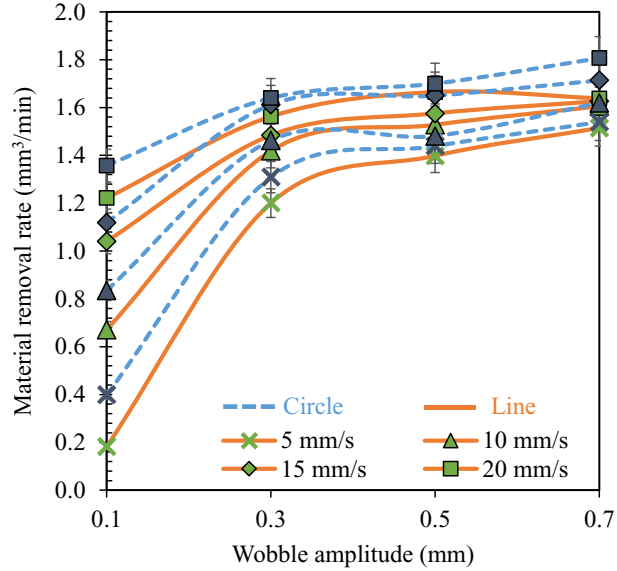


Figure 13: Material removal rate vs. wobble amplitude at different linear speeds (laser power: 10 W, number of passes: 10).

3.2.4. Number of passes

The investigated effects of the number of passes on the cut depth, kerf width, and surface roughness of the SiC samples are discussed in this section. The wobble amplitude and laser power are kept 0.5 mm and 10 W, respectively. The experiments were performed using the “linear” and “circle” wobble patterns. The first observed effect was a linear increase in both the cut depth and re-deposition height with the number of passes when using the “circle” pattern (see Fig. 10a). Reducing the linear speed was found to produce a similar effect on the cut depth as increasing the number of passes. Indeed, similar depths were obtained with 10 passes at 5 mm/s and 20 passes at 10 mm/s, or 40 passes at 10 mm/s and 80 passes at 20 mm/s. This can be explained by the fact that the MRR is proportional to the amount of the laser energy applied to a certain area for a given period of time. As a result, when the laser moves over an area two times faster, it would need to pass over that area twice.

Furthermore, when using the “circle” wobble pattern, the re-deposition height follows a similar trend linearly increasing with the number of passes (see Figs. 10a and b). However, when reaching 80 passes, the re-deposition height value does not vary much at different linear speeds, as it was observed in the case of 10-40 passes, and remains relatively constant at around 50 μm when increasing the laser speed from 10 mm/s to 20 mm/s. Therefore, at a very high number of passes, the relative material re-deposition increases with increasing speeds. This can be explained by the

fact that the use of the high number of passes results in very deep cuts, which impedes material removal and results in larger amounts of redeposits. This also explains a smaller kerf width formed at a higher number of passes – simply because a larger amount of the ablated material is being redeposited on the sides of the cut. As seen in Fig. 10c, for 80 passes using the “circle” pattern the kerf width is much smaller than the targeted 500 μm width for all the tested linear speed values becoming as small as 430 μm at 5 mm/s. The surface roughness of the cut produced using the “circle” pattern noticeably increases with the number of passes, as shown in Fig. 15. This could be explained by the larger amount of the evaporated material redeposited on the specimen surface in the form of particles and debris with some of them remaining on the surface of these deeper cuts. As the cuts become deeper, a larger number of these particles will not be able to escape and become entrapped within the cut trenches.

As seen in Fig. 14b, when using the “linear” wobble pattern, the effects of the number of passes on the depth/re-deposition height were very similar to those observed earlier for the “circle” pattern. The main differences were revealed for the values of the re-deposition height, which appear to be higher in general than those observed when using the “circle” pattern. Also, the surface roughness did not follow the same trend as that observed in the case of using the “line” pattern (see Fig. 14c). Both the re-deposition height values and the surface roughness of specimens cut using the “line” pattern were unusually high at the linear speed of 5 mm/s. Instead of observing a continuous increase in the surface roughness with the number passes in the studied range, the lowest surface roughness was observed at the number of passes of around 20. It was suggested that the laser beam was able to smoothen the specimen surface when increasing the number of passes from 10 to 20 in the case of using the “linear” pattern. It is possible that in general this particular pattern offers a less smooth movement when compared to the “circle” pattern and forms sharper straight cuts resulting in rough surfaces even when using a smaller number of passes.

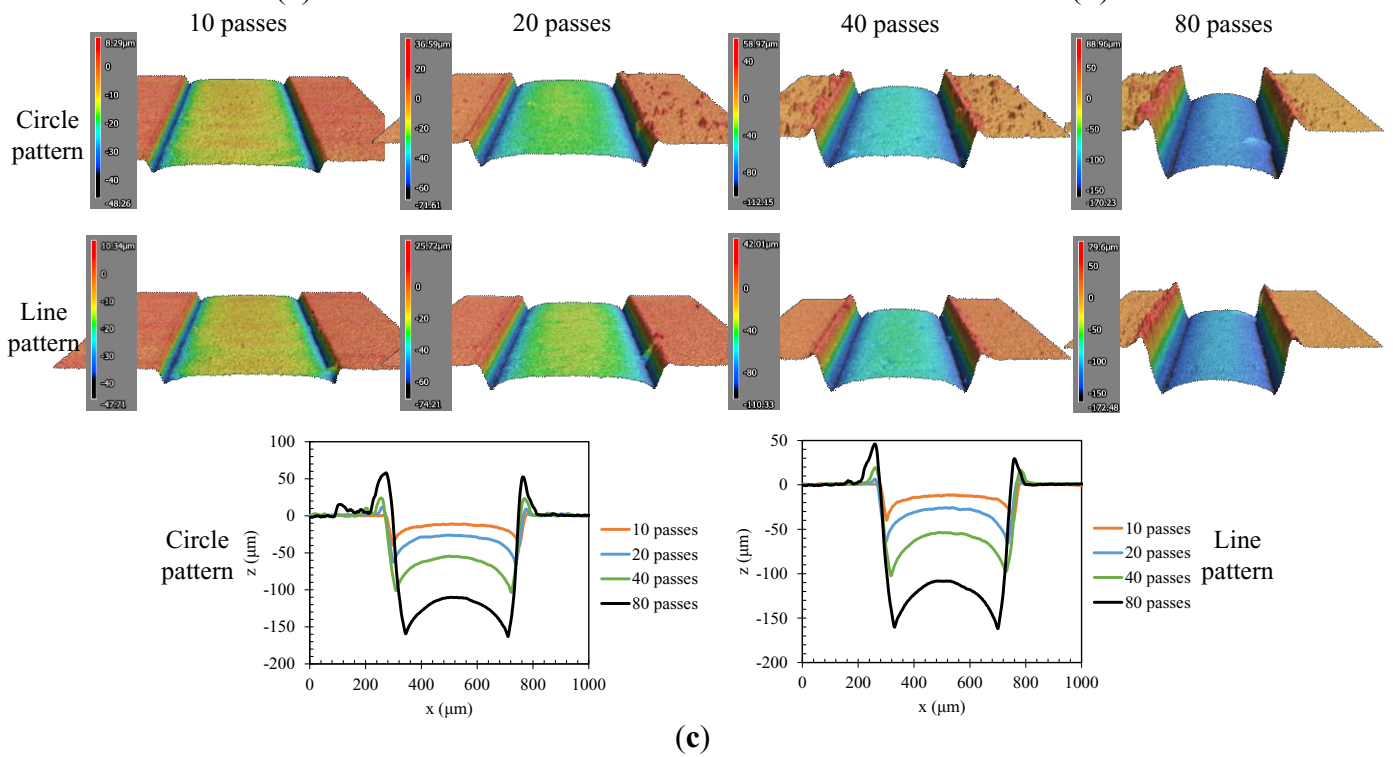
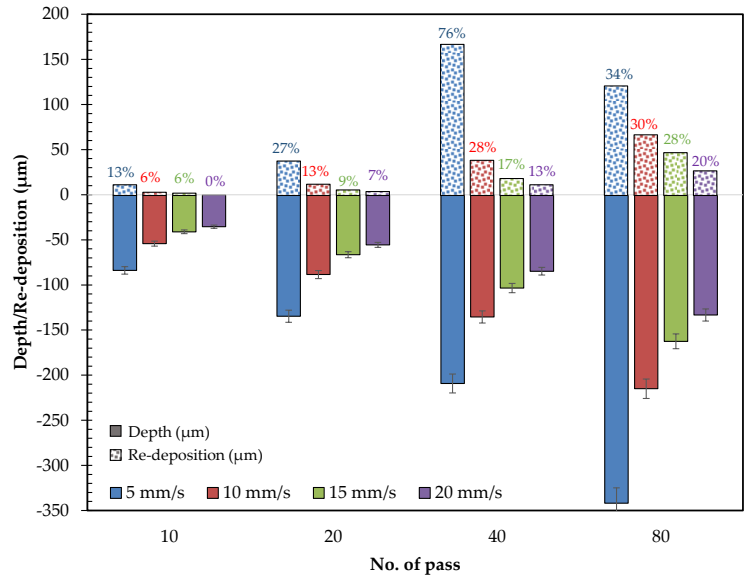
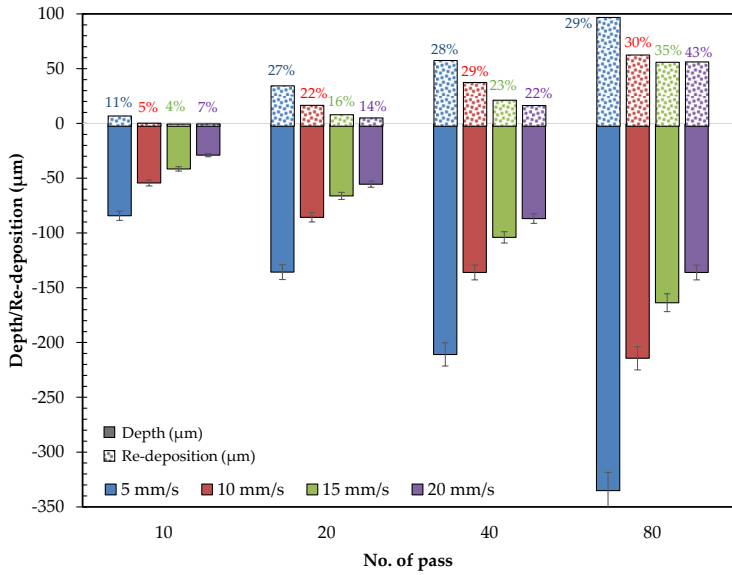


Figure 14: Depth/re-deposition vs. number of passes: (a) Circular wobble pattern, and (b) Linear wobble pattern. (c) 3D microscopy view of cuts with 10, 20, 40, and 80 passes at 15 mm/s (laser power: 10 W, wobble amplitude: 0.5 mm).

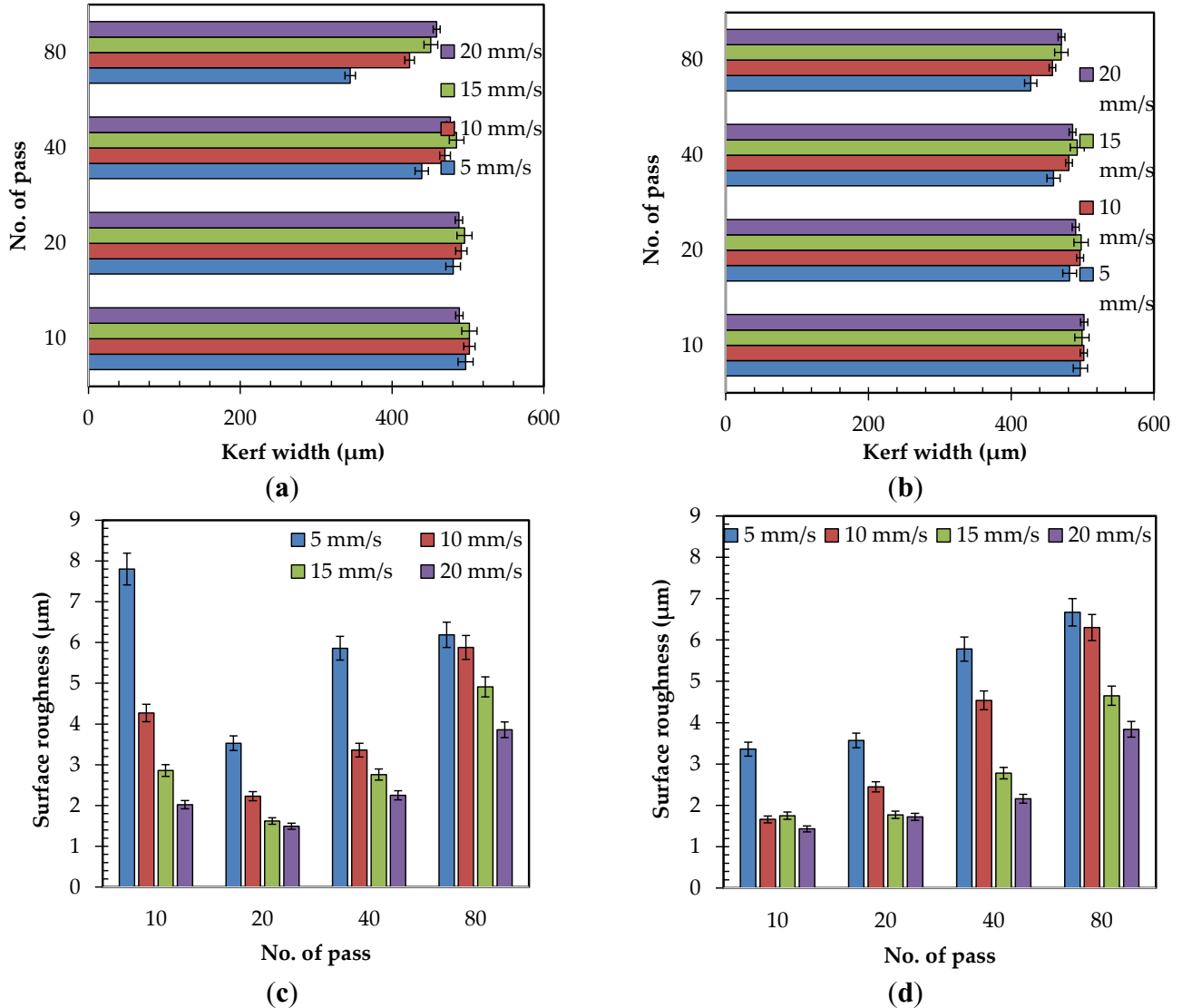
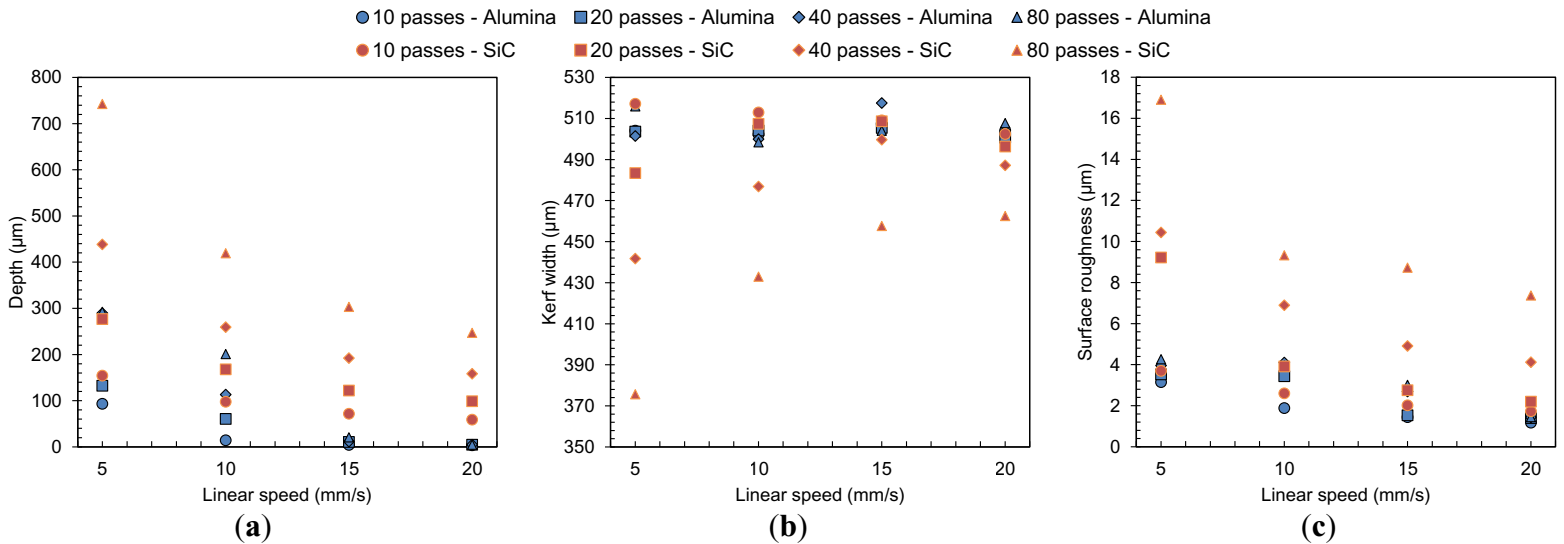


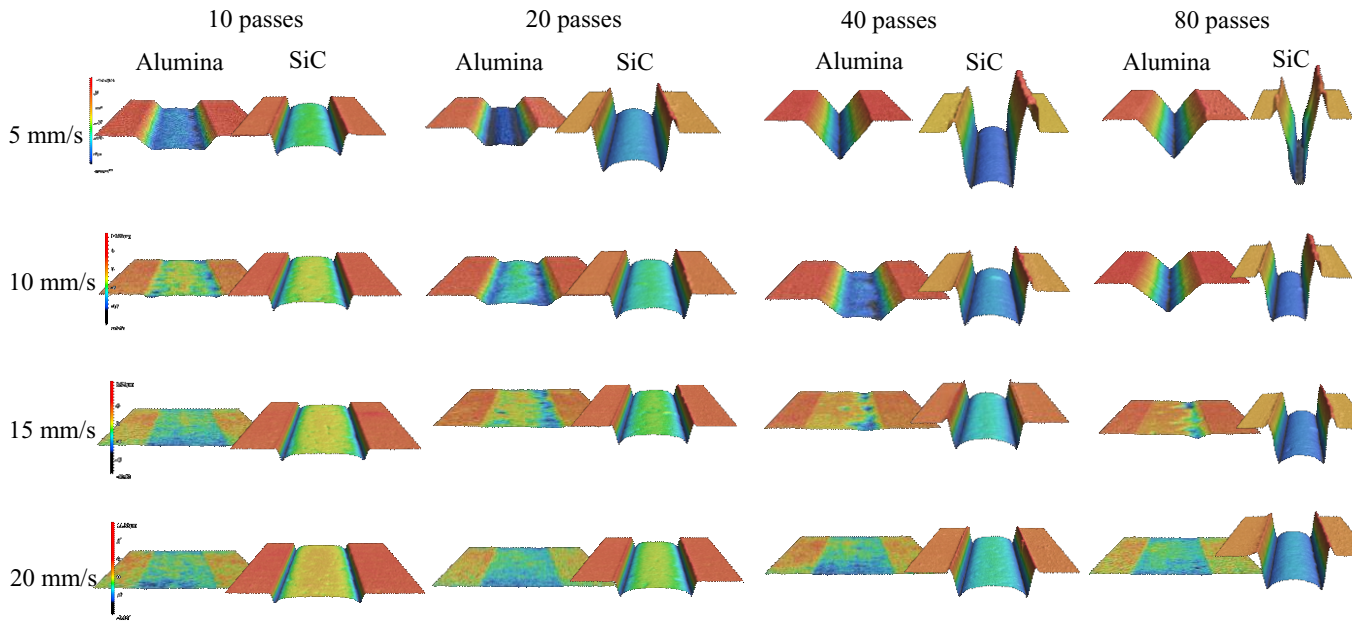
Figure 15: Kerf width and surface roughness vs. number of passes: (a), (c) “Circle” wobble pattern, and (b), (d) “Linear” wobble pattern (laser power: 10 W, wobble amplitude: 0.5 mm).

3.3. SiC laser cutting vs. alumina laser cutting

In order to further investigate characteristic features of laser ablation of SiC ceramics, a similar laser cutting procedure was applied to another ceramic material – alumina. The authors have investigated different effects of laser processing parameters on the shape and quality of alumina cuts [22, 37]. The wobble amplitude and laser power are kept 0.5 mm and 20 W, respectively. In general, the cuts produced in alumina were much shallower than those produced earlier in SiC using the same process parameters. This can be explained by the fact that the used alumina sheets were translucent (i.e., semi-transparent) whereas the SiC material was opaque. As a result, almost all the laser energy applied to the SiC specimen’s surface was used for material ablation. As seen

in Fig. 16a, at the laser linear speed of 15 mm/s and higher the laser was barely able to remove any material from the alumina surface. Even at 10 mm/s, more than 10 passes were needed to achieve any noticeable MRR. It was also noted that the alumina MRR followed a more linear trend with increasing energy density whereas the MRR of SiC increased in a more exponential fashion. This can be due to the fact that compared to alumina, SiC has a higher absorption coefficient and thermal conductivity. This can also explain a larger difference in the kerf widths for these two materials (Fig. 16b). As seen in Fig. 16c, SiC demonstrated more melting and re-deposition compared to alumina, clearly seen at high number of passes, which affected the kerf width. The higher re-deposition rate of SiC means that the material was being redeposited on the specimen surface adjacent to the cut as well as directly within the cut volume. As a result, the kerf width in the SiC shows significant changes with the linear speed value, especially large at 80 passes (Fig. 16b). On the contrary, the kerf width in alumina remains nearly unchanged in the entire range of linear speeds and used number of passes and congregates just above the targeted width of 500 μm . A similar behavior is demonstrated by the surface roughness, whose variation is less pronounced in alumina compared to SiC probably because it endures less re-deposition of coarse particles as well as less micro-cracks due to heating and expansion.





(d)

Figure 16: Comparison of SiC and alumina for different passes (10, 20, 40, and 80 passes) and linear speed (5, 10, 15, and 20 mm/s): (a) Depth, (b) Kerf width, and (c) Surface roughness. (d) 3D microscopy view of alumina and SiC cuts (laser power: 20 W, wobble amplitude: 0.5 mm).

4. Conclusions

In this study, various laser processing parameters were investigated in terms of their effect on the ablation of the reaction bonded SiC using a picosecond laser. According to the performed cross-sectional SEM, micro-Raman and GI-XRD analyses, the surface of the laser machined reaction bonded SiC material is covered with a re-deposited material of a thickness varying in the 2-10 μm range and consisting of an amorphous material with high oxygen content. The very top layer of the laser machined SiC surface is enriched with oxygen to a depth of about 3 μm . The sub-surface region in general retains its original 6H-SiC crystalline structure while the residual carbon in the reaction bonded SiC undergo volatilization.

The laser power and laser linear speed were found to be the most critical process parameters because they strongly affected the resulting depth, shape, and surface roughness of the produced cuts. Changing the linear speed proportionally changed the average power delivered per second per the surface area unit thereby affecting the MRR and the way in which the ablated material was removed. As a result of the study, the following laser cutting process conditions were identified as capable of producing deep, clean, and concise cuts in the SiC ceramics:

- Focal position: in order to produce deep cuts, the laser beam should be slightly out of focus with respect to the specimen surface in order to maximize the cut depth. Very deep cuts were

found to suffer from lower quality in terms of the amount of the redeposited material and surface roughness.

- The wobble feature: was found to be capable of increasing the size of the ablation areas at faster linear speeds. It was established that in order to achieve the minimum value of the re-deposition height, the ratio between the wobble frequency and the laser linear speed should be kept close to 80.
- The wobble pattern: It was found that in general, with small variations all the studied wobble patterns were capable of producing plausible results. “Circle” and “infinity” patterns produced cuts with lower relative re-deposition heights at low linear speeds while “linear” and “eight” patterns resulted in no material re-deposition at high linear speeds. When using “linear” and “eight” patterns, the kerf widths remained nearly unchangeable in a wide range of process parameters.
- Wobble amplitude: Varying the wobble amplitude had a strong effect on the cut depth, kerf widths, height of the redeposited material and the roughness of the machined surface. Deeper cuts offered smaller kerf widths at the cost of larger amounts of the redeposited material and increased surface roughness.
- Energy density controlled by the number of passes: Decreasing the energy density reduced the relative material re-deposition. However, at a high number of passes, the re-deposition sized increasing with further energy density increase. For the “line” pattern, the re-deposition height increased linearly with increasing energy densities showing no signs of reaching the limit.
- Ceramic material: At the same settings, the used picosecond laser was able to cut SiC to a larger depth than alumina because of the higher laser energy absorption of the latter, but resulted in a larger amount of the redeposited material and higher surface roughness.
- Higher re-deposition rate of SiC was usually accompanied by material melting rather than sublimation and generation of micro-cracks, which caused increase in the surface roughness and decrease in the kerf widths.
- High linear speeds are recommended for producing smooth shallow cuts in SiC ceramics.

Acknowledgment

The authors would like to thank the security, materials, and technologies (SMT) program at National Research Council Canada (NRC). The authors also acknowledge E. Poirier for his technical assistance in the laser processing.

References

1. Casady, J. and R.W. Johnson, *Status of silicon carbide (SiC) as a wide-bandgap semiconductor for high-temperature applications: A review*. Solid-State Electronics, 1996. **39**(10): p. 1409-1422.
2. Dong, H., et al., *Single crystalline 3C-SiC whiskers used for electrochemical detection of nitrite under neutral condition*. Ionics, 2016. **22**(8): p. 1493-1500.
3. Liu, S., et al., *Mild fabrication of SiC/C nanosheets with prolonged cycling stability as supercapacitor*. Journal of Materials Science & Technology, 2022. **110**: p. 178-186.
4. Zhou, L., et al., *Ultra-stable and durable piezoelectric nanogenerator with all-weather service capability based on N doped 4H-SiC nanohole arrays*. Nano-micro letters, 2022. **14**(1): p. 1-10.
5. Zhou, L., et al., *Piezoelectric nanogenerators with high performance against harsh conditions based on tunable N doped 4H-SiC nanowire arrays*. Nano Energy, 2021. **83**: p. 105826.
6. Gerhardt, R., *Properties and applications of silicon carbide*. 2011: BoD–Books on Demand.
7. Willander, M., et al., *Silicon carbide and diamond for high temperature device applications*. Journal of Materials Science: Materials in Electronics, 2006. **17**(1): p. 1-25.
8. Raynaud, C., *Silica films on silicon carbide: a review of electrical properties and device applications*. Journal of Non-Crystalline Solids, 2001. **280**(1-3): p. 1-31.
9. Kim, Y.-W., Y.-H. Kim, and K.J. Kim, *Electrical properties of liquid-phase sintered silicon carbide ceramics: a review*. Critical Reviews in Solid State and Materials Sciences, 2020. **45**(1): p. 66-84.
10. Sengupta, D., N. Quick, and A. Kar, *Laser conversion of electrical properties for silicon carbide device applications*. Journal of Laser Applications, 2001. **13**(1): p. 26-31.
11. Oliveros, A., A. Guiseppi-Elie, and S.E. Saddow, *Silicon carbide: a versatile material for biosensor applications*. Biomedical microdevices, 2013. **15**(2): p. 353-368.
12. Naslain, R., *Design, preparation and properties of non-oxide CMCs for application in engines and nuclear reactors: an overview*. Composites science and technology, 2004. **64**(2): p. 155-170.
13. Katoh, Y., et al., *Current status and recent research achievements in SiC/SiC composites*. Journal of Nuclear Materials, 2014. **455**(1-3): p. 387-397.
14. Somiya, S. and Y. Inomata, *Silicon carbide ceramics. 1. Fundamental and solid reaction*. Vol. 13. 1991: Springer.
15. She, X., et al., *Review of silicon carbide power devices and their applications*. IEEE Transactions on Industrial Electronics, 2017. **64**(10): p. 8193-8205.
16. Pecholt, B., S. Gupta, and P. Molian, *Review of laser microscale processing of silicon carbide*. Journal of Laser Applications, 2011. **23**(1): p. 012008.

17. Hocheng, H., W. Lei, and H. Hsu, *Preliminary study of material removal in electrical-discharge machining of SiC/Al*. Journal of Materials Processing Technology, 1997. **63**(1-3): p. 813-818.
18. Pawar, P., R. Ballav, and A. Kumar, *Machining processes of silicon carbide: a review*. Reviews on Advanced Materials Science, 2017. **51**(1): p. 62-76.
19. DeBastiani, D.L., M.F. Modest, and V.S. Stubican, *Mechanism of material removal from silicon carbide by carbon dioxide laser heating*. Journal of the American ceramic Society, 1990. **73**(7): p. 1947-1952.
20. Abrego Serrano, P.A., et al., *Spherical mirror and surface patterning on silicon carbide (SiC) by material removal rate enhancement using CO2 laser assisted polishing*. International Journal of Precision Engineering and Manufacturing, 2020. **21**(5): p. 775-785.
21. Islam, M., *An overview of research in the fields of laser surface modification and laser machining at the integrated manufacturing technologies institute, NRC*. Advanced Performance Materials, 1996. **3**(2): p. 215-238.
22. Beausoleil, C., et al., *Deep and high precision cutting of alumina ceramics by picosecond laser*. Ceramics International, 2020. **46**(10): p. 15285-15296.
23. Duan, L., et al., *Ablation of C/SiC-HfC composite prepared by precursor infiltration and pyrolysis in plasma wind tunnel*. Journal of Advanced Ceramics, 2020. **9**(3): p. 393-402.
24. Luan, X., et al., *Laser ablation behavior of Cf/SiHfBCN ceramic matrix composites*. Journal of the European Ceramic Society, 2016. **36**(15): p. 3761-3768.
25. Hamad, A.H., *Effects of different laser pulse regimes (nanosecond, picosecond and femtosecond) on the ablation of materials for production of nanoparticles in liquid solution*. 2016: IntechOpen London, UK.
26. Zheng, Q., et al., *Mechanism and morphology control of underwater femtosecond laser microgrooving of silicon carbide ceramics*. Optics Express, 2019. **27**(19): p. 26264-26280.
27. Wee, L.M., et al., *Solvent- Assisted Laser Drilling of Silicon Carbide*. International Journal of Applied Ceramic Technology, 2011. **8**(6): p. 1263-1276.
28. Iwatani, N., H.D. Doan, and K. Fushinobu, *Optimization of near-infrared laser drilling of silicon carbide under water*. International Journal of Heat and Mass Transfer, 2014. **71**: p. 515-520.
29. Duangwas, S., V. Tangwarodomnukun, and C. Dumkum, *Development of an overflow-assisted underwater laser ablation*. Materials and Manufacturing Processes, 2014. **29**(10): p. 1226-1231.
30. Valentini, F., et al., *Microstructure and Nanoindentation properties of surface textures obtained by laser machining and molding in silicon carbide*. Advanced Engineering Materials, 2013. **15**(5): p. 330-335.
31. Phipon, R., et al., *Laser beam micro engraving on silicon carbide*. Materials and Manufacturing Processes, 2020. **35**(12): p. 1372-1382.
32. Pan, Y., et al., *High-efficiency machining of silicon carbide Fresnel micro-structure based on improved laser scanning contour ablation method with continuously variable feedrate*. Ceramics International, 2021. **47**(3): p. 4062-4075.
33. Kasraei, S., et al., *Effect of CO2 and Nd: YAG lasers on shear bond strength of resin cement to zirconia ceramic*. Journal of Dentistry (Tehran, Iran), 2015. **12**(9): p. 686.
34. Lednev, V., et al., *Laser ablation comparison by picosecond pulses train and nanosecond pulse*. Laser Physics Letters, 2015. **12**(12): p. 126001.

35. Leone, C., S. Genna, and V. Tagliaferri, *An integrated approach for the modelling of silicon carbide components laser milling process*. The International Journal of Advanced Manufacturing Technology, 2021. **116**(7): p. 2335-2357.
36. Radmanesh, M., F. Ghanatir, and R. Radmanesh, *Comparing the efficacy of pulsed dye laser, Q-Switched Nd-YAG, CO₂, and combined CO₂ and Q-Switched Nd-YAG lasers for the treatment of cutaneous macular amyloidosis*. Journal of Dermatological Treatment, 2021. **32**(2): p. 258-260.
37. Esmail, I., et al., *Engineered net shaping of alumina ceramics using picosecond laser*. Optics & Laser Technology, 2021. **135**: p. 106669.
38. Sarvestani, H.Y., et al., *Architected ceramics with tunable toughness and stiffness*. Extreme Mechanics Letters, 2020. **39**: p. 100844.
39. Yazdani Sarvestani, H., et al., *Bioinspired stochastic design: tough and stiff ceramic systems*. Advanced Functional Materials, 2022. **32**(6): p. 2108492.
40. Autruffe, A., et al., *Indentation behaviour of interlocked structures made of ice: Influence of the friction coefficient*. Advanced Engineering Materials, 2007. **9**(8): p. 664-666.
41. Nakashima, S.-i. and H. Harima, *Raman investigation of SiC polytypes*. physica status solidi (a), 1997. **162**(1): p. 39-64.
42. Madito, M., T. Hlatshwayo, and C. Mtshali, *Chemical disorder of α -SiC layer induced in 6H-SiC by Cs and I ions co-implantation: Raman spectroscopy analysis*. Applied Surface Science, 2021. **538**: p. 148099.
43. Wang, F., et al., *Microstructures and mechanical properties of α -SiC ceramics after high-temperature laser shock peening*. Journal of the American Ceramic Society, 2022. **105**(4): p. 2411-2420.
44. Okumura, H., et al., *Raman scattering of SiC: Application to the identification of heteroepitaxy of SiC polytypes*. Journal of applied physics, 1987. **61**(3): p. 1134-1136.
45. Schade, M., et al., *High-resolution investigations of ripple structures formed by femtosecond laser irradiation of silicon*. Analytical and bioanalytical chemistry, 2010. **396**(5): p. 1905-1911.
46. Cheng, Q., et al., *Si quantum dots embedded in an amorphous SiC matrix: nanophase control by non-equilibrium plasma hydrogenation*. Nanoscale, 2010. **2**(4): p. 594-600.
47. Burton, J., et al., *Spatial characterization of doped SiC wafers by Raman spectroscopy*. Journal of Applied Physics, 1998. **84**(11): p. 6268-6273.